JMEPEG (2016) 25:3375–3383
DOI: 10.1007/s11665-016-2074-8 ©The Author(s). This article is published with open access at Springerlink.com
1059-9495/$19.00

Thermal and Microstructure Characterization of Zn-Al-Si Alloys and Chemical Reaction with Cu Substrate During Spreading

Katarzyna Berent, Janusz Pstruś, and Tomasz Gancarz

(Submitted November 15, 2015; in revised form April 13, 2016; published online April 28, 2016)

The problems associated with the corrosion of aluminum connections, the low mechanical properties of Al/Cu connections, and the introduction of EU directives have forced the potential of new materials to be investigated. Alloys based on eutectic Zn-Al are proposed, because they have a higher melting temperature (381 °C), good corrosion resistance, and high mechanical strength. The Zn-Al-Si cast alloys were characterized using differential scanning calorimetry (DSC) measurements, which were performed to determine the melting temperatures of the alloys. Thermal linear expansion and electrical resistivity measurements were performed at temperature ranges of −50 to 250 °C and 25 to 300 °C, respectively. The addition of Si to eutectic Zn-Al alloys not only limits the growth of phases at the interface of liquid solder and Cu substrate but also raises the mechanical properties of the solder. Spreading test on Cu substrate using eutectic Zn-Al alloys with 0.5, 1.0, 3.0, and 5.0 wt.% of Si was studied using the sessile drop method in the presence of QJ201 flux. Spreading tests were performed with contact times of 1, 8, 15, 30, and 60 min, and at temperatures of 475, 500, 525, and 550 °C. After cleaning the flux residue from solidified samples, the spreadability of Zn-Al-Si on Cu was determined. Selected, solidified solder/substrate couples were cross-sectioned, and the interfacial microstructures were studied using scanning electron microscopy and energy dispersive x-ray spectroscopy. The growth of the intermetallic phase layer was studied at the solder/substrate interface, and the activation energy of growth of Cu_5Zn_8, $CuZn_4$, and CuZn phases were determined.

Keywords microstructure, spreading, thermal and mechanical properties, Zn-Al-Si

1. Introduction

The Zn-Al eutectic system has been proposed as an alternative to soldering at high-temperatures, with a maximum working temperature is up to 350 °C (Ref 1). This alloy has many desirable characteristics, including low cost, high mechanical properties, and good thermal and electrical conductivities. However, the Zn-Al alloy demonstrates very weak wettability of substrates and oxidation resistance, which could be eliminated by the addition of Cu (Ref 2), Ag (Ref 3), and Mg (Ref 4). Many authors have investigated the effects of different chemical and metallurgical aspects on the impact properties of Zn-Al alloys (Ref 2-9). In this study, the effects of Si addition on the microstructure and mechanical properties of the Zn-Al alloy were examined.

However, the mechanical properties of the binary Zn-Al alloys are not suitable for most engineering applications. Silicon is the most important alloying element used in the majority of cast alloys (Ref 9). It is responsible for a good castability (due to its high fluidity), it has very low solubility in aluminum alloys, and therefore it precipitates as virtually pure Si particles, which improve the strength. A small addition of Si caused stress resistance to increase in the tensile test (Ref 6, 7). Si content also led to increased wear resistance and hardness (Ref 7, 8) in Zn-Al-Si alloys. Jian et al. (Ref 9) showed that the wear rate of alloys containing 2 wt.% silicon instead of copper was approximately 10 times lower than the wear rate of the Zn27Al alloy.

The possibility of using Zn-Al alloys to solder Al/Cu (Ref 10), Al/Mg (Ref 11), Al/steel (Ref 12), and Cu/Cu (Ref 13) extend their applications in industry. However, there are few studies showing the impact of temperature and time on phenomena occurring at the interface of liquid solder and the solid substrate. In (Ref 14), Al/Cu and Cu/Cu joints soldered by eutectic Zn-Al are shown; from Cu side, three intermetallic compounds (IMCs) from the Cu-Zn system of CuZn, Cu_5Zn_8, and $CuZn_4$ phases were present at the interface. The addition of Ag and Cu to Zn-Al alloys (Ref 2, 3, 14, 15) caused the growth of the IMC layer at the interface to be blocked. According to the results of this work, the effects of Si addition on the kinetics of formation and growth of the CuZn, Cu_5Zn_8, and $CuZn_4$ phases in the spreading process were studied.

This article is an invited submission to JMEP selected from presentations at the Symposium "Wetting and High-Temperature Capillarity," belonging to the Topic "Joining and Interfaces" at the European Congress and Exhibition on Advanced Materials and Processes (EUROMAT 2015), held on September 20-24, 2015, in Warsaw, Poland, and has been expanded from the original presentation.

Katarzyna Berent, AGH University of Science and Technology, Academic Centre for Materials and Nanotechnology, Krakow, Poland; and **Janusz Pstruś** and **Tomasz Gancarz**, Institute of Metallurgy and Materials Science, Polish Academy of Sciences, Krakow, Poland. Contact e-mails: kasia.berent@gmail.com and kberent@agh.edu.pl.

2. Experimental

The cast alloys of Zn-Al with 0.5, 1.0, 3.0, and 5.0 wt.% of Si were prepared in a glove box filled with high purity Ar (99.9999 vol.%), from equally high purity 99.999% of Al, Si, and Zn elements in Al_2O_3 crucibles. The samples for electrical resistivity tests were sucked into quartz capillaries, and for the mechanical tests were casted into graphite molds. Spreading tests on Cu substrate of eutectic Zn5.3Al alloys with 0.5, 1.0, and 3.0 wt.% of Si were performed using the sessile drop (SD) method. A more detailed description of the experimental apparatus can be found in the earlier work of Moser et al. (Ref 18). Spreading tests were carried out in the presence of QJ201 flux and without protective atmosphere at temperatures of 475, 500, 525, and 550 °C, in order to determine the activation energy of the phase forming. Therefore, flux QJ201 from powder, consisting of KCl 50, LiCl 32, NaF 10, and $ZnCl_2$ 8 (wt.%), was applied for the purposes of protection and oxide removal. In order to determine the kinetics of growth of the IMCs, the tests were performed at 500 °C for spreading times of 1, 8, 15, 30, and 60 min. As described in (Ref 2, 3), the spreading areas of 0.5 g samples of Zn-Al-Si solder were calculated after cleaning the flux residue from solidified samples, and the spreadability of Zn-Al-Si alloys on Cu was determined in accordance with ISO 9455-10:2013-03. Selected solder/substrate couples were cut perpendicular to the plane of the interface on a diamond wire saw, mounted in conductive resin, ground, polished, and subjected to microstructure and elemental analysis using FEI Quanta 3D FEG scanning electron microscope (SEM) coupled with energy dispersive x-ray spectrometry (EDS), in order to study the interfacial microstructure and the IMCs occurring at interface, the same as described in (Ref 2, 3). The SEM-EDS measurements were performed at an accelerating voltage of 15 kV. The growth rate and activation energy of CuZn, Cu_5Zn_8, and $CuZn_4$ layers in the solid state were determined. Thermal analysis of Zn-Al-xSi alloys was carried out at temperatures up to 500 °C in an argon gas flow at 40 mL/min, with a heating rate of 10 °C/min, using differential scanning calorimetry (DSC). The alloys were measured to verify the CTE and thermal deformation in the temperature range from −50 to 250 °C, with a heating rate of 5 °C/min under a helium 5 N gas flow of 20 mL/min, using a thermal mechanical analyzer (TMA). Electrical resistivity measurements were made using the four-point method with a Keithley 6220 as the current source (output 100 mA with an accuracy of 10 µA) coupled with a Keithley 2182 nanovoltmeter (10 mV range with an accuracy of 1nV) at temperatures ranging from 25 to 300 °C, with heating steps of 10 °C during a 180 min under air. The mechanical properties of the Zn-Al-Si alloys were evaluated using an INSTRON 6025 testing machine modernized by Zwick/Roell.

3. Results and Discussion

3.1 Characteristics of Cast Alloys

3.1.1 Microstructures. The microstructures of the Zn-Al-xSi alloys in the as-cast state consist mainly of three phases. One has a bright contrast, the second has a lighter gray color, and the third is darker, as shown in Fig. 1. EDS analysis was carried out on these points. The phase with bright contrast (point A) is a zinc-rich phase containing about 98.9 wt.% Zn.

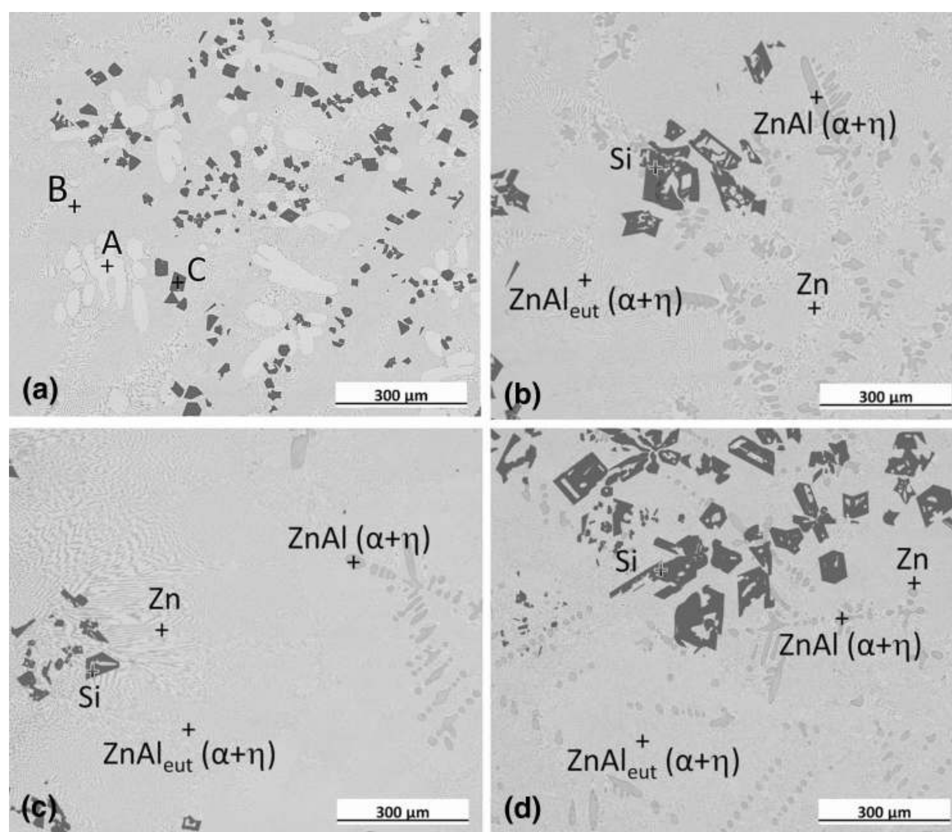

Fig. 1 Microstructure of the as-cast Zn-Al alloys with different amounts of Si: (a) 0.5, (b) 1.0, (c) 3.0, and (d) 5.0 wt.%

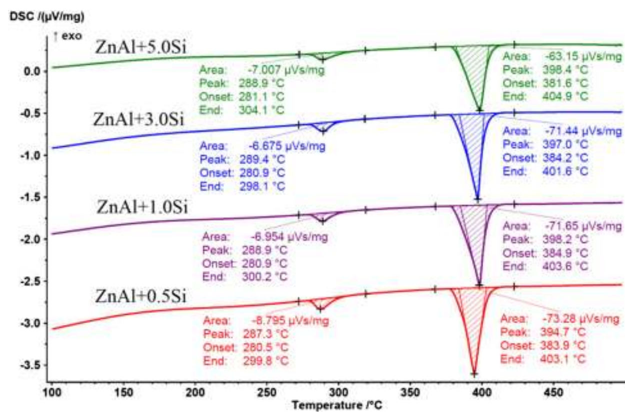

Fig. 2 The DSC curves of the Zn-Al-xSi as-cast alloys

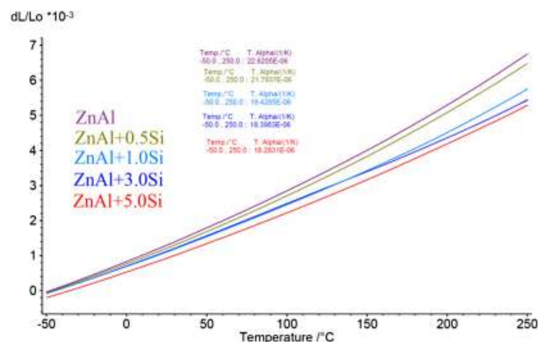

Fig. 3 TMA results of thermal expansion measurements vs. temperature

The gray eutectic phase (point B) was found to be an aluminum-rich phase containing about 22.4 wt.% Al. In addition, some particles with darker appearance (point C) were observed at different places containing only Si. The addition of silicon had not formed the IMCs, only caused occurring Si particles on the microstructure of the Zn-Al alloy. The solubility of silicon in the zinc-aluminum matrix is nearly zero (Ref 20). Therefore, silicon solidifies into the primary and eutectic silicon particles in the microstructure of the Zn-Al-Si alloys (Ref 6-9). The distribution of Si particles is non-uniform in the alloys. As can be seen in Fig. 1(a-c), the microstructure of Zn-Al-Si consists of eutectic colonies of an Al-rich phase and Zn-rich phase formed at the eutectic and Si particles. In the Zn-Al-0.5Si alloy, the microstructure displays primary crystals of the Zn phase with a dendritic morphology, and an $\alpha + \eta$ eutectic phase distributed in the interdendritic space (Fig. 1a). The primary Zn phases were surrounded by eutectic phases, in which fine eutectic Si platelets were found to be dispersed in eutectic Zn matrix. The silicon particles are smaller, and their distribution is more uniform, compared to the other alloys. As illustrated in Fig. 1(b)-(d), when 1.0-5.0 wt.% Si is added to the Zn-Al matrix, in the eutectic Zn-Al microstructure increasing amount of Si particles. The composition of the light contrasted areas indicates a Zn-rich phase (η-Zn), and the darker areas represent the Al-rich phase. Additionally, an Al-Zn-rich compound occurs at the expense of the Zn-rich phase. With increased silicon content, the size of the Si particles also increases, and their distribution becomes non-uniform. The eutectic silicon particles can be seen in the area of the Zn-rich phase and the phase mixture for all alloys. Similar observations were determined by Vencl et al. (Ref 8), where the primary Zn area increased with decreasing Si content.

3.1.2 Thermal Properties. The DSC melting curves of Zn-Al-xSi alloys are presented in Fig. 2. The addition of Si had inconsiderable on the melting temperature of Zn-Al-xSi solder. The DSC results demonstrated two obvious endothermic peaks for the Zn5.3Al-Si solder alloys. The two peaks indicated two steps in the melting process of Zn-Al-Si solder. Based on the Zn-Al-Si phase diagram (Ref 15), for the first endothermic peak, at ~281 °C, the first reaction was a solid solution from the α- to the α'-phases, where the reaction of the Al-rich face-centered cubic (fcc) and hexagonal close-packed (hcp) phase was observed to convert to a Zn-rich phase of fcc crystal structure. The second endothermic peak appeared at ~384 °C, where the reaction was melting of eutectic Zn-Al. The addition of silicon to alloys causes slight differences between melting and solidification temperature. As shown in Fig. 2, increasing the concentration of silicon contributes to an increased melting point. According to Takaku et al. (Ref 15) and Gancarz et al. (Ref 2, 3), all Zn-Al solders show two endothermic peaks, and both reactions take place at approximately the same temperature.

3.1.3 Thermal Expansion. Increasing electrical power density requires solder with excellent mechanical properties, high reliability, and stability, because higher electric power results in higher heat flux and, therefore, leads to a higher operating temperature for electronic equipment. The thermal expansion mismatch between components grows larger due to differences in their coefficients of thermal expansion (CTE), and causes a great enough strain in solder to induce fatigue failure mode (Ref 1). The results of thermal expansion measurements are shown in Fig. 3. The CTE was calculated in the present study at the range of -50 to 250 °C. At the beginning, the thermal expansion coefficients of all Zn-Al-xSi solders are essentially the same value, although the values are significantly lower than for eutectic Zn-Al solder. The CTE are 21.79, 19.43, 18.38, and 18.29 ($\times 10^{-6}$ K^{-1}) for 0.5, 1.0, 3.0, and 5.0 wt.% Si, respectively, showing that the CTE decreases as Si content increases. The Zn-Al-Si alloys have lower CTE than Zn-Al alloys (22.6×10^{-6} K^{-1}) and Pb-based solder alloys (30.0×10^{-6} K^{-1}). In their complementary work, Gancarz et al. (Ref 16) found that the thermal expansion was higher for Zn-Al-In than for Pb-5Sn, despite the fact that the In dissolves in Zn-Al and does not create an IMC. In the case of Zn-Al-Si alloys, reducing CTE by increasing Si content reduces differences between Cu (16.9×10^{-6} K^{-1}) (Ref 19) and solder, causing fewer cracks in working joints during temperature changes.

3.1.4 Electrical Resistivity. The temperature dependence of the electrical resistivity (ρ) for the Zn-Al-Si solders was measured, as shown in Fig. 4. As can be seen, the resistivity of Zn-Al-Si alloys increases linearly with increasing temperature. Alloys with high silicon content exhibit higher electrical resistance. The values of resistivity measurements range from 7.2 to 7.6 μΩ cm at room temperature. This can be related to the microstructure of the sample. The presence of a higher amount of the eutectic phase is the reason of higher electrical resistivity. Gancarz et al. (Ref 3, 16) found that the electrical resistivity of Zn-Al-In and Zn-Al-Ag increases as temperature rises and different metal components are added: from 6.5 to 8.5 μΩ cm at room temperature for Zn-Al-xIn (x = 0.5-1.5 wt.%) and 6.5-7.2 μΩ cm for Zn-Al with addition of Ag

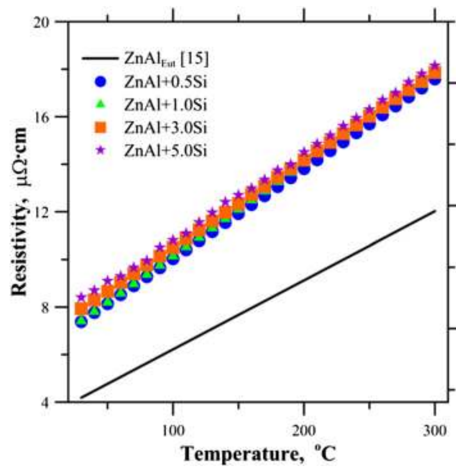

Fig. 4 Electrical resistivity of Zn-Al alloys with different Si contents

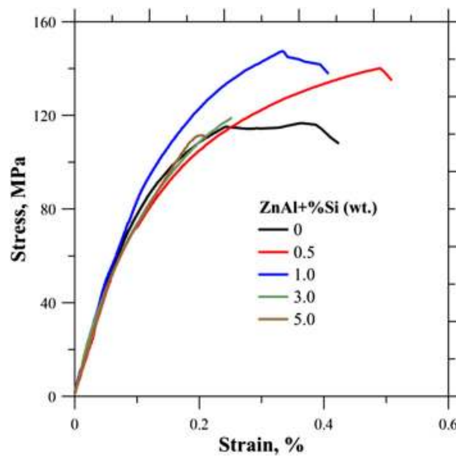

Fig. 5 The stress-strain curves of Zn-Al-xSi solder alloy

from 0.5 to 1.5 wt.%. But all values are greater than the values of ρ obtained for the eutectic Zn-Al alloy (5.0 μΩ cm), and lower than those of a Sn-37Pb solder (14.25 μΩ cm) (Ref 16).

3.1.5 Mechanical Properties. Tensile test was used to evaluate the mechanical properties of the as-cast Zn-Al-Si alloys compared with the strength of eutectic ZnAl solder. Figure 5 shows the stress-strain curve of Zn-Al-Si alloys. It was found that the tensile strength of Zn-Al-Si alloys increased with increasing silicon content above 1.5 wt.% (Ref 17). The alloys with 0.5 and 1.0 wt.% Si content showed sufficiently high tensile strength of 144 and 147 (MPa), respectively. When the amount of silicon increases above 5.0 wt.%, the tensile strength decreases. The brittleness of coarse silicon crystals (both eutectic and primary silicon) is the main reason for the poor mechanical properties of ZA alloys. The strength of Zn-Al-3.0Si and Zn-Al-5.0Si alloys is greatly reduced, to 118 and 110 (MPa), respectively. The elongation to failure of Zn-Al-Si alloys was very low, even lower than that for Pb-5Sn (39%), and had an effect on the preparation of samples, and the condition and temperature treatment of samples after casting. The tensile properties correlated to the microstructural behavior as a function of element contents. This may be related to a change of eutectic composition with the increase of silicon content and the creation of primary Si particles. Savaskan et al. (Ref 6) show that the addition of a small amount of Si into Zn15Al-Cu alloys can greatly enhance their mechanical

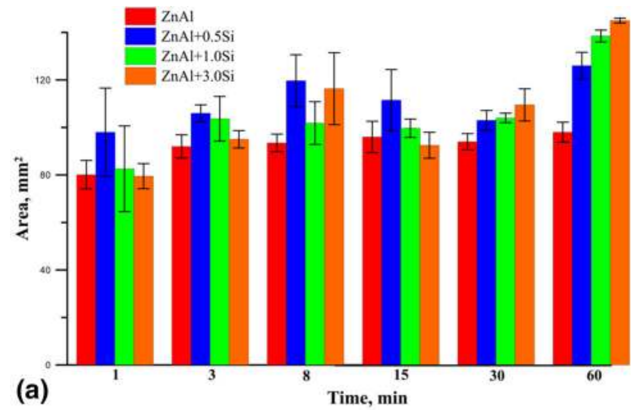

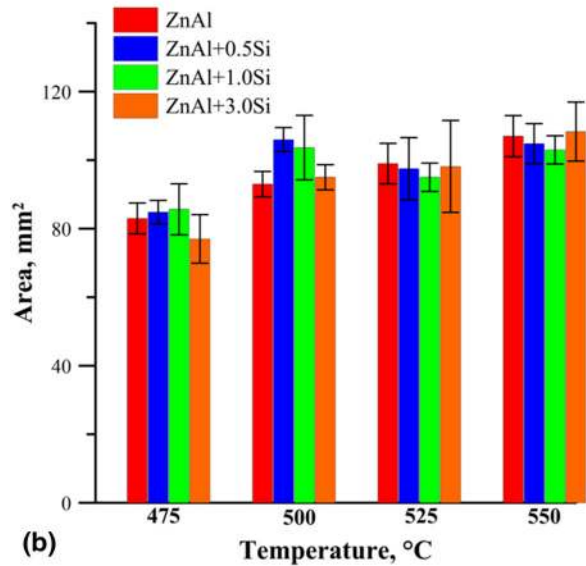

Fig. 6 Effect of silicon on spreading area of ZnAl solder on Cu substrate for different (a) times, (b) temperatures

Table 1 The results of EDS analysis of the IMC layers formed at the Zn-Al-Si/Cu

IMCs	Cu (at.%)	Zn (at.%)
Zn-Al-0.5Si		
β-CuZn	48.8 ± 1.0	51.2 ± 1.0
γ-Cu_5Zn_8	41.0 ± 0.8	59.0 ± 1.2
ε-$CuZn_4$	19.5 ± 0.8	80.5 ± 1.2
Zn-Al-1.0Si		
β-CuZn	48.9 ± 1.0	51.1 ± 1.0
γ-Cu_5Zn_8	42.3 ± 0.9	57.7 ± 1.2
ε-$CuZn_4$	19.6 ± 0.8	80.4 ± 1.6
Zn-Al-3.0Si		
β-CuZn	47.4 ± 1.0	52.6 ± 1.1
γ-Cu_5Zn_8	42.3 ± 0.9	57.7 ± 1.2
ε-$CuZn_4$	21.0 ± 0.4	79.0 ± 1.6

properties. This result shows that silicon can be an alternative element to cooper. When the content of silicon is more than 1 wt.%, it was found that the trend reverses.

3.1.6 Spreading Test. Results of the spreading area *A* of Zn-Al-xSi alloys on Cu substrate after different times of contact (1, 8, 15, 30, and 60 min) and temperatures (475, 500, 525, and 550 °C) are shown in Fig. 6(a)-(b). The droplet area of the molten Zn-Al-xSi alloys is larger than those of the eutectic Zn-Al alloy. The maximum spreading area was obtained for Zn-Al-0.5Si for varying periods of time ranging from 1 to 15 min. The spreading area of Zn-Al-0.5 Si was 98 mm^2 for 1 min. For 1.0 and 3.0 wt.% Si content, the area of contact is lower than those for 0.5 wt.% Si content, being 82 and 79 mm^2 for 1 min. For these two compositions, the increase of time from 30 to 60 min

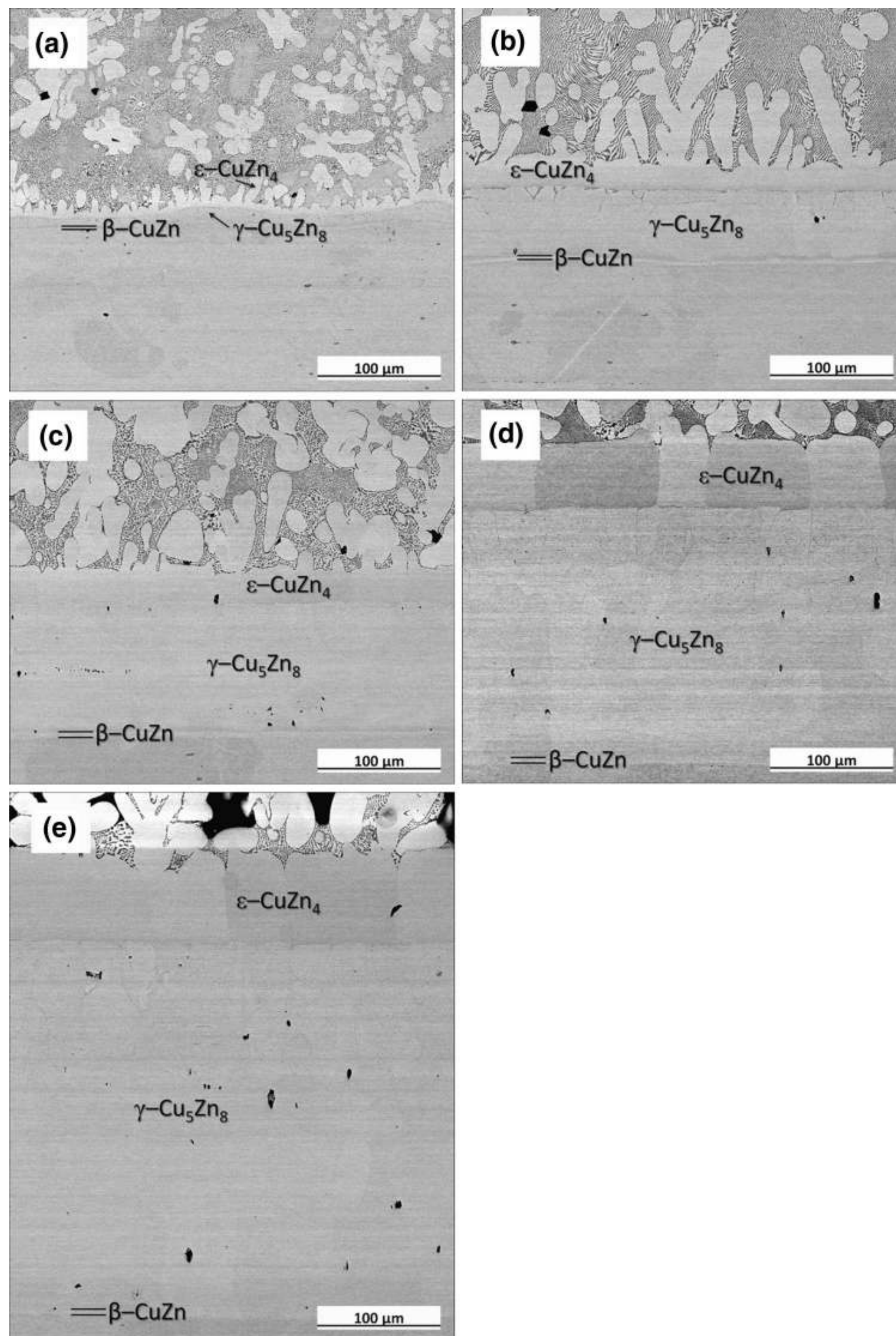

Fig. 7 Backscattered SEM micrographs showing the microstructure of IMCs between Zn-Al-0.5Si and Cu substrate at 500 °C at different times: (a) 1 (b) 8, (c) 15, (d) 30, and (e) 60 min, respectively

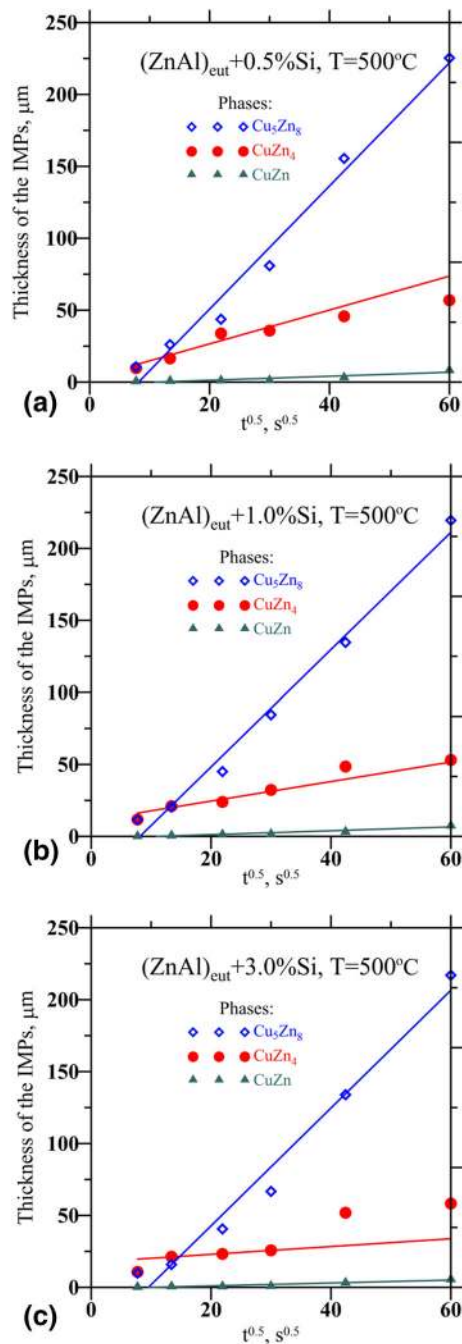

Fig. 8 Plots of thickness vs. square root of time for IMCs formed at interfaces in the Zn-Al-xSi/Cu samples during the reflow process at 500 °C for: (a) 0.5, (b) 1.0, and (c) 3.0 wt.% Si

results in higher contact area. However, further increase of time to 30 min leads, for Zn-Al-0.5Si, to a insignificant decrease of area. As contact time increased, the spreading area increased slowly.

Figure 6b shows that the spreading area of the alloys increased as the temperature increased from 475 to 550 °C. At 475 °C, additional Si content, up to 1 wt.%, resulted in a decreasing spreading area. A further temperature increase, to 525 °C, causes the area to decrease, and a temperature of 550 °C affects the growth of contact area from 95 to 103 mm^2 for Zn-Al-1.0Si. It is shown that eutectic Zn-Al and Zn-Al-3.0Si have higher areas at 525 and 550 °C. Increasing Si content up to 1 wt.% in the solder may lead to decreasing the spreading time of solder. It has to be noted that, with increasing temperature and time, the solder spreadability is improved, and the best results were obtained at 550 °C. However, the spreadability of Zn-Al-Si is relatively poor compared to the high lead solder due to the oxygen affinity of Zn and Al. The addition of a small amount of Cu and Ag to ZA solder was investigated by Gancarz et al. (Ref 2, 3). It was observed that the spreading area obtained for eutectic ZnAl with Cu increased with increasing time, temperature, and Cu content. This can be compared to with the spreading area of Zn-Al with Ag, where the effect of time was very small, whereas the effect of temperature on spreading area was strong. Generally, the addition of Ag reduced the spreading area (Ref 3), but this effect was rather smaller compared to the increased spreading area in Zn-Al with Si alloys.

3.1.7 Effect of Time on Chemical Reaction at Interface During Spreading. One of the present authors (Ref 3, 21) reports that three Cu-Zn intermetallic compound layers were formed at 500 °C, and that the processes occurring at the solder/substrate interface can be divided into three distinct stages. The first one involves the dissolution of copper by liquid zinc, the second the crystallizations, and the third the solid-state transformations. After the spreading treatment, the consumption of the Cu substrate by Zn was observed, and it was noted that three reaction layers (ε-$CuZn_4$, γ-Cu_5Zn_8, and β-CuZn) at the interface were formed, between the Zn-Al-xSi alloys and Cu substrate. The formation of these layers was confirmed by Takaku et al. (Ref 15) and Gancarz et al. (Ref 2, 3, 16). The Zn-Al-based alloys are exceptional alloys forming peculiar IMCs with Cu due to the presence of Zn, with dissolving inside Al, which is in accordance with phase diagram Al-Cu-Zn (Ref 22). This is due to the fact that the highest growth of the IMC phase with time and temperature correlates to the stability of phases from the Al-Cu-Zn system (Ref 3). The ThermoCalc calculations show that the γ-phase that is Cu_5Zn_8 and Al_4Cu_9 (in the phase diagram of Al-Cu-Zn) has the lowest Gibbs free energy. However, considering the time of the spreading process, the amount and availability of components are controlled by diffusion of Cu and Zn to the interface. Figure 7 shows backscattered electron (BSE) micrographs of the microstructure of Zn-Al-0.5Si solder at 500 °C, at times of (a) 1, (b) 8, (c) 15, (d) 30, and (e) 60 min. A thin layer of CuZn forms close to the Cu side, a scallop-shaped $CuZn_4$ layer forms at the solder side, and a Cu_5Zn_8 layer forms in the middle. The average thickness of layers was measured for different reflowing times. Inside the Cu_5Zn_8 layer, the fast path of Cu diffusion is shown, which is also observed in Zn-Al with Ag and Cu alloys (Ref 3, 15, 21). The results of EDS quantitative analysis are summarized in Table 1. The composition of the three phases coincides well with the $CuZn_4$, Cu_5Zn_8, and CuZn phase, even for the thicker one. As the content of Si increased, the fraction of the $CuZn_4$ phase decreased (due to the diffusion of Zn toward the solder interface and controlled growth of interfacial IMCs). After eight minutes reflow, it was observed that the IMCs increased in thickness with reflow time. However, the growth rates of IMC layers had been somewhat reduced for the samples with higher Si content. The effect of Cu and Ag on the microstructure is in good agreement with results from previous studies in the most popular Zn-Al cast alloys (Ref 3), although there are inconsistencies in the influence of Si on the thickness of IMC (Ref 2, 3).

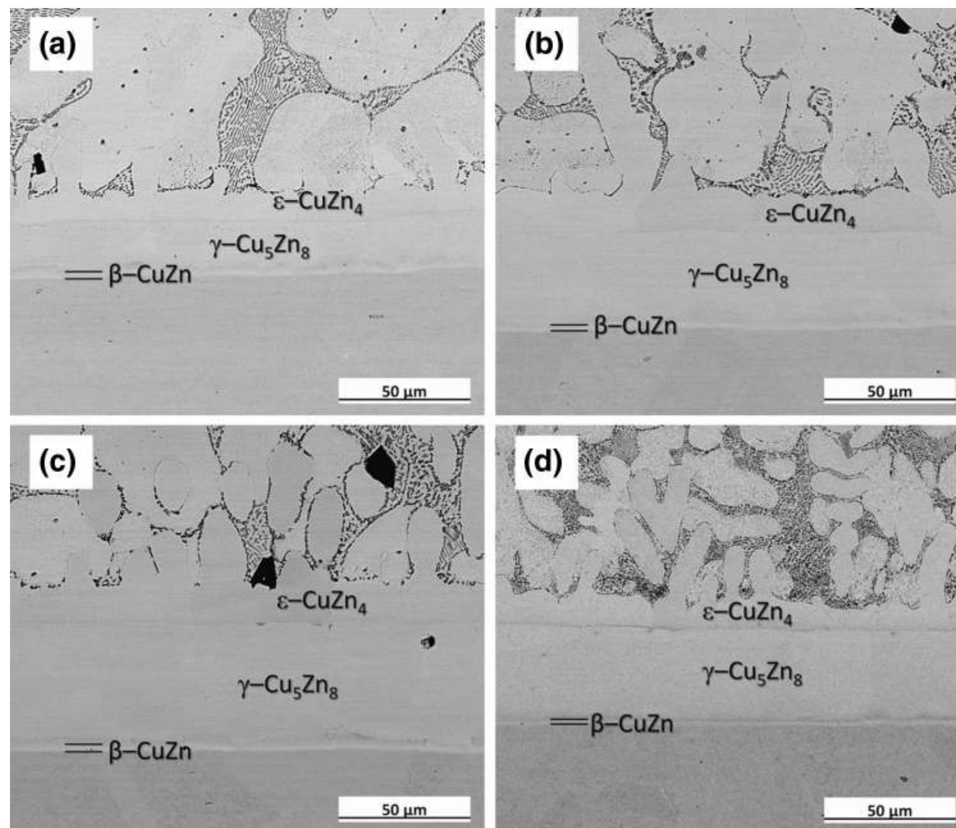

Fig. 9 Backscattered SEM micrographs showing the microstructure of IMCs between Zn-Al-0.5Si and Cu substrate after 8 min at different temperatures: (a) 475 (b) 500, (c) 525, and (d) 550 °C, respectively

It was found that, when the Ag and Cu concentration was low (0.5 wt.%), the thickness of the interface layers was the smallest (Ref 3, 15).

3.1.8 Intermetallic Compound Thickness Analysis. Figure 8(a), (b), and (c) presents the thickness of IMC layers formed at interface in temperature 500 °C and the time from 1 to 60 min, for Zn-Al with Si addition of 0.5, 1.0, and 3.0 wt.%, respectively. In the beginning of spreading test from 1 to 8 min, the thickness of Cu_5Zn_8 and $CuZn_4$ layers is almost the same, and after 15 min, the highest thickness was obtained for Cu_5Zn_8. Generally, at the interface of Zn-Al solder with a Cu substrate, the three binary IMCs $CuZn_4$, Cu_5Zn_8, and CuZn are observed, which is in accordance with the phase diagram of Al-Cu-Zn. Taking into account the thickness of IMC layers and relationship between d (the IMC thickness) and t (time), the character of diffusion could be determined:

$$\delta = kt^n,$$

where k represents the growth rate coefficient for the consumption rate (experimental values). This means that the growth rate constant k was determined from the slope of the linear relation in Fig. 8. The possibility description of time by square root are respond to the formation of the IMC layers for all investigated solders which is controlled by volume diffusion.

Takaku et al. (Ref 15) have reported that the addition of 1 wt.% Cu to Zn-Al alloy causes activation energy to decrease and enhances the growth of the IMC layers. Different results were observed by Gancarz et al. (Ref 3), who confirmed that the addition of 0.5 wt.% Ag to Zn5.3Al solder could effectively reduce the thickness of Cu_5Zn_8 and $CuZn_4$ layers by lowering the diffusion rate of Zn in the Cu substrate. Grain boundary diffusion plays a major role in the formation of the new phase, compared to surface or bulk diffusion. Hence, the large primary Si particles that appeared near to the eutectic region and within the Zn matrix act as barriers to Cu and Zn diffusion along the grain boundaries to form Cu-Zn IMCs. The average thickness of each IMC layer was measured for different times. Longer times correspond to greater IMC thickness. The thin β-CuZn layer was also reported in the literature (Ref 2, 3, 15).

3.1.9 Effect of Temperature on Chemical Reaction at Interface During Spreading. Figure 9 present a series of backscattered electron images illustrating the effect of temperature on the microstructure of the Zn-Al-0.5Si solder, after the spreading test for a time of 8 min. Changes in the thickness and shape of the IMCs were registered at four different temperatures (475, 500, 525, and 550 °C). The microstructure of Zn-Al-Si solder (Fig. 9) shows three IMC layers, $CuZn_4$, Cu_5Zn_8, and CuZn, which are formed at the Cu substrate-solder interface for all levels of Si content in Zn-Al alloys. The CuZn intermetallic layer grows immediately on Cu substrate. The morphology of $CuZn_4$ is a scallop-shaped layer, while those of Cu_5Zn_8 and CuZn are flat. The thin β-CuZn layer varies from about 0.4 to 1.5 µm, the γ-Cu_5Zn_8 layer from about 15.1 to 39.5 µm, and the ε-$CuZn_4$ layer from about 11.5 to 26.2 µm for Zn-Al-0.5Si, depending on temperature. Such reaction morphologies are quite similar to those of Zn-Al-Cu and Zn-Al-Ag (Ref 2, 3). For the present reaction layers, it can be said that Cu

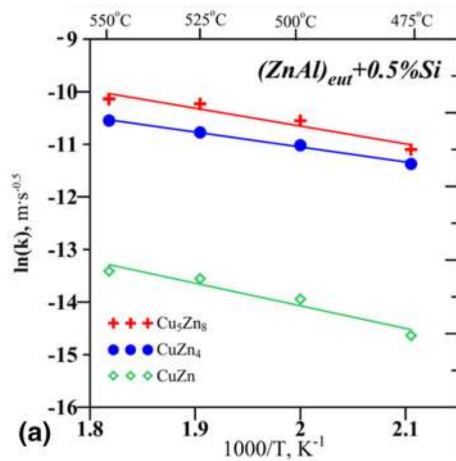

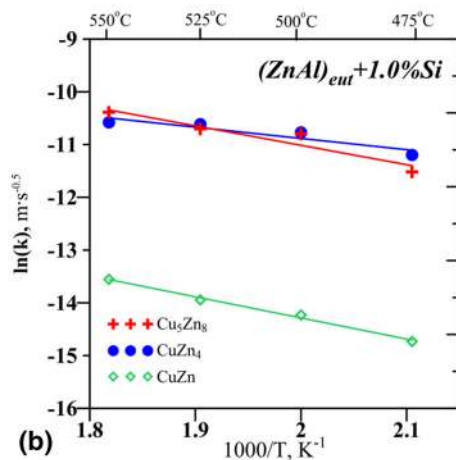

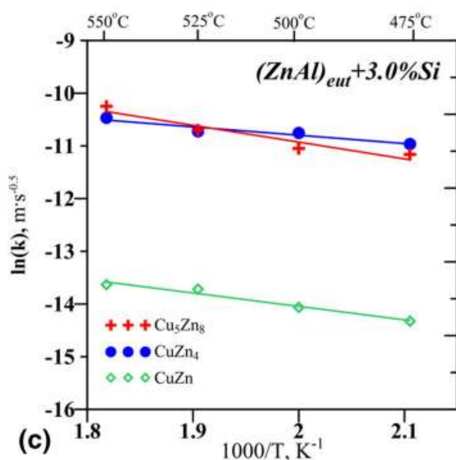

Fig. 10 Arrhenius plot for the growth of the total interfacial Zn-Al-xSi solder for (a) 0.5, (b) 1.0, and (c) 3.0 wt.% Si

dissolution into the liquid solder forms the scallop-shaped $CuZn_4$ layer. In this case, the Cu is predominantly transported to molten solder along the $CuZn_4$ grain boundaries during spreading. Higher spreading temperatures correspond to thicker IMCs.

Table 2 The activation energy of IMCs of ZnAl alloys with Si content after spreading

Alloys (wt.%)	IMCs	Activation energy Q, kJ/mol
Zn-Al (Ref 2)	CuZn	32.38
	Cu_5Zn_8	42.38
	$CuZn_4$	29.54
Zn-Al-0.5Si	CuZn	35.77
	Cu_5Zn_8	28.18
	$CuZn_4$	23.65
Zn-Al-1.0Si	CuZn	33.27
	Cu_5Zn_8	30.62
	$CuZn_4$	17.34
Zn-Al-3.0Si	CuZn	21.18
	Cu_5Zn_8	26.50
	$CuZn_4$	13.15

3.1.10 Kinetics of Growth of the IMC Layers. Since IMC growth is a diffusion-dominated process, the growth rate for interface migration can be described by an Arrhenius equation as follows:

$$k = k_0 \cdot \exp^{-\frac{Q}{RT}},$$

where k_0 is the migration rate constant, Q is the activation energy, R is the universal gas constant, and T is the absolute temperature. Figure 10 shows the *ln k* versus ($1/T$) plots for individual phases for Zn-Al alloys with Si addition of 0.5, 1.0, and 3.0 wt.%, respectively. The activation energy values were calculated from the slopes of the Arrhenius plot using a linear regression model derived from Fig. 10(a)-(c). The activation energies of Zn-Al-Si are summarized in Table 2. The slops of the lines in Fig. 10 suggest higher activation energy for γ-Cu_5Zn_8 and β-CuZn than for ε-$CuZn_4$. Accordingly, it can be predicted that the first intermetallic phase to be formed at the interface between the Zn solder and Cu substrate is $CuZn_4$. The apparent activation energies calculated for the growth of β, γ, and ε were 33.27, 30.62, and 17.34 kJ/mol for Zn-Al-1.0Si are similar to those of Zn-Al-1.0Cu (Ref 15), at 48, 36, and 16 kJ/mol, respectively. However, slightly lower compare to eutectic Zn-Al alloy for β, γ, and ε were 32.38, 42.38, and 29.54 kJ/mol (Ref 3). As the activation energy of IMCs increases, the formation and growth of this compound becomes more difficult. On the other hand, low activation energies indicate easier IMC formation and growth. Addition of less than 3.0 wt.% Si to eutectic Zn-Al increases the activation energy of IMCs which inhibits their nucleation and growth. Data obtained by Gancarz et al. (Ref 2), for a Zn-Al-Cu/Cu interface, show lower activation energy than the data collected by Takaku (Ref 15). In line with (Ref 3), the addition of Ag to eutectic Zn-Al also increases activation energy to 49, 37, and 17 kJ/mol for β, γ, and ε, respectively. In all cases, the addition of a small amount of metal content increases the activation energy of IMCs, which inhibits the nucleation and growth of IMC layers.

4. Conclusion

The present study is concerned with the effects of silicon addition on the microstructures, and electrical and mechanical

properties of Zn-Al solder alloys. The following conclusions can be drawn:

1. The microstructure of cast alloys consists of both eutectic and primary Si particles. For Zn-Al alloys containing less than 1.0 wt.% Si, the microstructure was blocky and showed a homogeneous distribution of primary particles. The eutectic Si had a mostly fibrous morphology, which became much larger in size in the alloys containing more than 1.0 wt.% Si.
2. The DSC results demonstrated that the addition of 0.5, 1.0, 3.0, and 5.0 wt.% Si changes the melting temperatures slightly. Melting occurred over a slightly higher range of temperatures.
3. From TMA analysis, the linear average coefficient of thermal expansion (CTE) was found. Meanwhile, a small amount of 0.5-1.0 wt.% Si, added to a eutectic ZnAl alloy, results in an appreciable change in thermal and mechanical properties.
4. The results of electrical resistivity measurements show that the addition of Si to eutectic ZnAl increases the electrical resistivity in the range from 7.2 to 7.6 μΩ cm at room temperature for Zn-Al-xSi (x = 0.5-3.0 wt.%).
5. Tensile test results indicate that adding a small amount of Si can clearly improve the strength and ductility, but the trend reverses above 1.0 wt.%. The decrease in tensile strength can be explained by the increased amount of large silicon particles.
6. The formation of three IMC layers, such as CuZn, Cu_5Zn_8, and $CuZn_4$, was observed at the solder/Cu substrate interface. The results show that the addition of Si can reduce the activation energy of the intermetallic phases. But the growth rate of the $CuZn_4$ phase decreased due to the diffusion of Zn toward the solder interface and the growth of interfacial IMCs was controlled by the amount of Si. The IMC layers became thinner as Si content increased. As shown earlier, the spreadability and the thickness of the IMC layers increase at higher temperatures and longer spreading times.
7. The experimental results presented in this paper demonstrated that a small amount of silicon causes general refinement of microstructure and better mechanical properties.

Acknowledgment

This work was financed by the Minister of Science and High Education of Poland Grant IP2014 011473, in the years 2015 to 2017.

Open Access

This article is distributed under the terms of the Creative Commons Attribution 4.0 International License (http://creativecommons.org/licenses/by/4.0/), which permits unrestricted use, distribution, and reproduction in any medium, provided you give appropriate credit to the original author(s) and the source, provide a link to the Creative Commons license, and indicate if changes were made.

References

1. G. Zeng, S. McDonald, and K. Nogita, Development of High-Temperature Solders: Review, *Microelectron. Reliab.*, 2012, **52**, p 1306–1322
2. T. Gancarz, J. Pstrus, S. Mosinska, and S. Pawlak, Effect of Cu Addition to Zn-12Al Alloy on Thermal Properties and Wettability on Cu and Al Substrate, *Metall. Mater. Trans. A*, 2016, **47**, p 368–377
3. T. Gancarz, J. Pstruś, P. Fima, and S. Mosinska, Effect of Ag Addition to Zn-12Al Alloy on Kinetics of Growth of Intermediate Phases on Cu Substrate, *J. Alloys Compd.*, 2014, **582**, p 313–322
4. W. Jurczak, Wpływ litu na właściwości i odporność korozyjną stopów Al-Zn-Mg w wodzie morskiej, *Zeszyty Naukowe Akademii Marynarki Wojennej, ROK XLVI, nr*, 2005, **3**, p 162 (in Polish)
5. X. Yan, S. Liu, W. Long, J. Huang, L. Zhang, and Y. Chen, The Effect of Homogenization Treatment on Microstructure and Properties of ZnAl15 Solder, *Mater. Des.*, 2013, **45**, p 440–445
6. T. Savaskan and A. Hekimoglu, Microstructure and Mechanical Properties of Zn-15Al-Based Ternary and Quaternary Alloys, *Mater. Sci. Eng., A*, 2014, **603**, p 52–57
7. T. Savaskan and A. Aydmer, Effects of Silicon Content on the Mechanical and Tribological Properties of Monotectoid-Based Zinc-Aluminium-Silicon Alloys, *Wear*, 2004, **257**, p 377–388
8. A. Vencl, I. Bobic, F. Vucetić, B. Bobic, and J. Ruzic, Structural, Mechanical and Tribological Characterization of Zn25Al Alloys with Si and Sr Addition, *Mater. Des.*, 2014, **64**, p 381–392
9. L. Jian, E.E. Laufer, and J. Masounave, Wear in Zn-Al-Si Alloys, *Wear*, 1993, **165**, p 51–56
10. F. Ji, S. Xue, J. Lou, Y. Lou, and S. Wang, Microstructure and Properties of Cu/Al Joints Brazed with Zn-Al Filler Metals, *Trans. Nonferrous Met. Soc. China*, 2012, **22**, p 281–287
11. L. Ma, D.Y. He, X.Y. Li, and J.M. Jiang, High-Frequency Induction Soldering of Magnesium Alloy AZ31B Using a Zn-Al Filler Metal, *Mater. Lett.*, 2010, **64**, p 596–598
12. Y. Jinlong, X. Songbai, X. Peng, L. Zhaoping, D. Wei, and Zh Junxiong, Development of Novel CsF-RbF-AlF3 Flux for Brazing Aluminium to Stainless Steel with Zn-Al Filler Metal, *Mater. Des.*, 2014, **64**, p 110–115
13. M. Prach and R. Kolenak, Soldering of Copper with High-Temperature Zn-Based Solders, *Procedia Eng.*, 2015, **100**, p 1370–1375
14. J. Pstrus and T. Gancarz, Interfacial Phenomena in Al/Al, Al/Cu, and Cu/Cu Joints Soldered Using an Al-Zn Alloy with Ag or Cu Additions, *J. Mater. Eng. Perform.*, 2014, **23**, p 1614–1624
15. Y. Takaku, L. Felicia, I. Ohnuma, R. Kainuma, and K. Ishida, Interfacial Reaction Between Cu Substrates and Zn-Al Base High-Temperature Pb-Free Solders, *J. Electron. Mater.*, 2008, **37**, p 314–323
16. T. Gancarz, J. Pstrus, P. Fima, and S. Mosinska, Thermal Properties and Wetting Behavior of High Temperature Zn-Al-In Solders, *J. Mater. Eng. Perform.*, 2012, **21**, p 599–605
17. T.J. Chen, C.R. Yuan, M.F. Fu, Y. Ma, Y.D. Li, and Y. Hao, *Mater. Sci. Technol.*, 2008, **24**, p 1321–1332
18. Z. Moser, P. Fima, K. Bukat, J. Sitek, J. Pstrus, W. Gasior, M. Koscielski, and T. Gancarz, Investigation of the Effect of Indium Addition on Wettability of Sn-Ag-Cu Solders, *Solder. Surf. Mt. Tech.*, 2011, **23**, p 22–29
19. S.M. Spearing, M.A. Tenhover, D.B. Lukco, L. Viswanathan, and D.K. Hollen, Models for Thermomechanical Behavior of Metal/Ceramic Laminates, *Mat. Res. Soc. Symp. Proc.*, 1994, **323**, p 128
20. E.A. Brandes, Ed., *Smithells Metals References Book*, VI, ed., Butterworth, London, England, 1983
21. J. Pstrus, P. Fima, and T. Gancarz, Wetting of Cu and Al by Sn-Zn and Zn-Al Eutectic Alloys, *J. Mater. Eng. Perform.*, 2012, **21**, p 606–613
22. V. Raghavan, Al-Cu-Zn, *J. Phase Equilib. Diff.*, 2007, **28**, p 183–188